

Fermi velocity spectrum and incipient magnetism in TiBe_2

T. Jeong, A. Kyker, and W. E. Pickett

Department of Physics, University of California, Davis, California 95616, USA

(Received 20 October 2005; revised manuscript received 12 December 2005; published 14 March 2006)

We address the origin of the incipient magnetism in TiBe_2 through precise first principles calculations, which we find to overestimate the ferromagnetic tendency and, therefore, require correction to account for spin fluctuations. TiBe_2 has sharp fine structure in its electronic density of states, with a van Hove singularity only 3 meV above the Fermi level. Similarly to the isovalent weak ferromagnet ZrZn_2 , it is the positioning of flat bands along the K - W - U lines of hexagonal face of the fcc Brillouin zone that make the system prone to magnetism, and more so if electron carriers are added. We find that the Moriya B coefficient [multiplying ω/q in the fluctuation susceptibility $\Delta\chi(q, \omega)$] is divergent when the velocity vanishes at a point on the Fermi surface, which is very close (3 meV) to occurring in TiBe_2 . In exploring how the ferromagnetic instability (the $q=0$ Stoner enhancement is $S \approx 60$) might be suppressed by fluctuations in TiBe_2 , we calculate that the Moriya A coefficient (of q^2) is negative, so $q=0$ is not the primary instability. Explicit calculation of $\chi_o(q)$ shows that its maximum occurs at the X point $(1, 0, 0) 2\pi/a$. TiBe_2 is, therefore, an incipient *antiferromagnet* rather than ferromagnet as has been supposed. We further show that simple thermal smearing of the peak accounts for most of the temperature dependence of the susceptibility, which previously had been attributed to local moments (via a Curie-Weiss fit), and that energy dependence of the density of states also strongly affects the magnetic field variation of the susceptibility.

DOI: 10.1103/PhysRevB.73.115106

PACS number(s): 71.18.+y, 75.10.Lp, 71.20.-b, 71.28.+d

I. INTRODUCTION

The cubic Laves compound TiBe_2 was already shown 40 years ago to have quite unusual behavior of the magnetic susceptibility $\chi(T)$ and the Knight shift.¹ χ^{-1} showed a strong increase with lowering temperature but a clear deviation from Curie-Weiss form, while the Knight shift was temperature dependent and negative. The magnetic properties of TiBe_2 have been controversial since Matthias *et al.*² interpreted the susceptibility peak at 10 K in TiBe_2 as itinerant antiferromagnetism (AFM) with an associated magnetic moment of $1.64\mu_B$, and Stewart *et al.* reported a transition at 2 K that seemed characteristic of magnetic ordering.

However, a clear picture has emerged gradually after the idea of weak itinerant antiferromagnetism had been abandoned because of the subsequent lack of experimental evidence.^{3,4} Many experiments have shown that TiBe_2 is instead a strongly enhanced paramagnet⁵⁻⁷ and undergoes a metamagnetic transition⁸⁻¹⁰ (field-driven ferromagnetism) around 5.5 T. Also one can see similarity to the magnetic behavior of Ni_3Ga by comparing the values of the low-temperature susceptibility, $\chi = 1.65 \times 10^{-2}$ emu/mole for Ni_3Ga ,¹¹ and $\chi = 0.90 \times 10^{-2}$ emu/mole for TiBe_2 .² Based on the magnetization data of Monod *et al.*,⁶ Wohlfarth⁹ suggested the transition at 5.5 T should be first order. Wohlfarth's considerations received at least partial support from theoretical band-structure considerations coupled with the de Haas-van Alphen data of van Deursen *et al.*¹²

Clarity began to arise with the extensive experiments of Acker *et al.* who interpreted their magnetization data⁵ in fields to 21 T and the magnetization data of Monod *et al.*⁶ as evidence for exchange-enhanced paramagnetism or spin fluctuations in TiBe_2 . They found the system $\text{TiBe}_{2-x}\text{Cu}_x$ to become FM at a critical concentration

$x_{cr} = 0.155$. Stewart *et al.*¹³ measured the specific heat of TiBe_2 ($\gamma = 42$ mJ/mole K^2) at low temperature in 0 and 7 T and interpreted the behavior as evidence of spin fluctuations.

The isoelectronic isostructural material ZrZn_2 is considered a classic example of an weak itinerant ferromagnet. Magnetic measurements find very small magnetic moments (values from $0.12\mu_B$ to $0.23\mu_B$),^{14,15} hence the characterization as a weak ferromagnet. The magnetization of ZrZn_2 increases substantially with the field, but unlike TiBe_2 with its metamagnetic transition, the increase continues smoothly to fields as high as 35 T. The Curie temperature T_C drops approximately linearly with pressure, from 29 K at $P=0$ to 4 K at $P=16$ kbar, which extrapolates to a quantum critical point (QCP) at $P=18-20$ kbar. The report of superconductivity coexisting with ferromagnetism (FM) in ZrZn_2 near this¹⁶ QCP enlivened both theoretical and experimental attention, but more recently it has been shown¹⁷ there is no bulk superconductivity. TiBe_2 , on the other hand, has been addressed only rarely for the past 20 years.

The complex temperature-field behavior of TiBe_2 has led to many speculations about the microscopic mechanisms. Of course, spin fluctuations play a central part, and the highly enhanced susceptibility suggests this system is near a quantum critical point (at slightly enlarged lattice constant, say, as well as for the Cu alloying). If FM fluctuations dominate, then a metamagnetic transition (field-driven FM state) around 5 T would make sense. If AFM fluctuations dominate, application of a field suppresses the fluctuations, providing another way to interpret specific heat under the applied field.¹⁸ The anomalies in the conduction electron spin resonance (CESR) linewidth¹⁹ around 2 K have been interpreted in terms of a thermal spontaneous magnetism,^{20,21} and a decrease in the resistivity is also seen at that temperature.⁵ All of these scenarios are sensitive to the Fermi surface

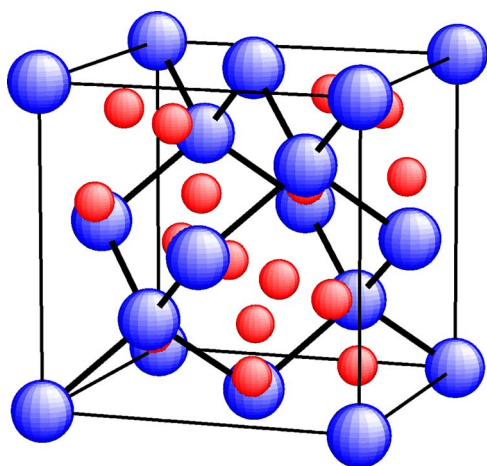


FIG. 1. (Color online) The cubic Laves C15 structure of TiBe_2 , shown in the unit cube. The Ti atoms (large spheres) form a diamond structure sublattice. The Be (small spheres) sit in interstitial sites and form a sublattice of vertex-sharing tetrahedra (the pyrochlore lattice).

shape, velocity spectrum, and possibly the energy dependence of the density of states near the Fermi energy, and it is these questions that we address in this paper.

Band-structure intricacies by themselves also can come into play. Shimizu showed²⁰ that an independent electron system with magnetic coupling can undergo a first-order transition to a “spontaneous thermal magnetism” state (within a range $T_1 < T < T_2$) if it is highly enhanced and if the Fermi level lies within a local minimum in the density of states. The effects of magnetic fluctuations should of course be added²² to the free energy of both the ordered and disordered phases to make this treatment more realistic.

Local-density approximation (LDA) energy band studies of TiBe_2 have been reported previously.^{23–25} Those studies revealed a split narrow peak in the density of states (DOS) $N(E)$ near the Fermi energy (E_F), with calculated Stoner factors $IN(E_F)$ greater than unity, giving the Stoner instability to FM. Here, I is the Stoner exchange interaction averaged over the Fermi surface. Thus, as for a few cases that have come to light more recently,^{26,27} ferromagnetism is incorrectly predicted, indicating the need to account for magnetic fluctuations not included in LDA that will suppress magnetic ordering. By comparing the calculated value of $N(E_F)$ with the measured susceptibility, a Stoner enhancement $S = [1 - IN(E_F)]^{-1} \approx 60$ was obtained, making TiBe_2 a more strongly exchange-enhanced metal than Pd.

All of these calculations, carried out 25 years ago, used shape approximations for the density and potential, and for a detailed investigation of the weak ferromagnetism precise electronic structure methods are required. In this work, the precise self-consistent full-potential linearized-augmented-plane-wave (FLAPW) method and full-potential local-orbital (FPLO) minimum-basis band-structure scheme are employed to investigate thoroughly the electronic and magnetic properties of TiBe_2 based on the density functional theory. We compared and checked the calculation results of the both methods. We consider the effect of magnetism on the band structure, Fermi surface, and Fermi velocity and compare

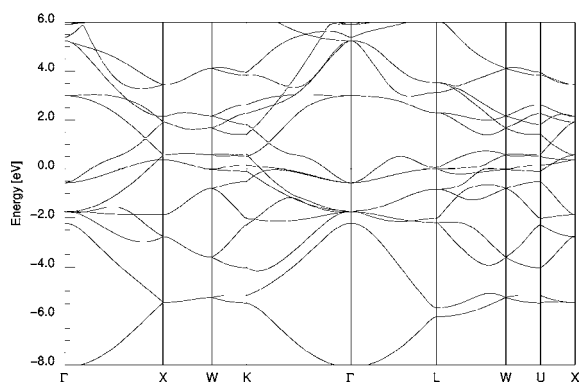


FIG. 2. The full LDA band structure of nonmagnetic TiBe_2 along symmetry lines showing that there are several bands near the Fermi level (taken as the zero of energy) with weak dispersion; they are primarily Ti $3d$ in character.

with experiments and previous band calculations.

II. CRYSTAL STRUCTURE

TiBe_2 crystallizes into a cubic Laves phase C15 crystal structure (Fig. 1). The C15 (AB_2) structure is a close packed structure and the site symmetry is high for the two constituents. Ti atoms occupy the positions of a diamond sublattice while the Be atoms form a network of interconnected tetrahedra, with two formula units per primitive cell. Since the major contributions to $N(E_F)$ come from Ti, the local environment of Ti atoms may be important to keep in mind. Each Ti is surrounded by 12 Be neighbors at a distance of 2.66 Å and tetrahedrally by four Ti neighbors at a distance 2.78 Å away. The TiBe_2 structure belongs to the $Fd\bar{3}m$ space group with Ti occupying the $8a$ site and Be the $16d$ site. The site symmetry of Ti is $\bar{4}3m$ (tetrahedral) and Be has $\bar{3}m$ site symmetry. The atomic positions are symmetry determined, and we used experimental lattice constant 6.426 Å for all calculations.

III. METHOD OF CALCULATIONS

We have applied the full-potential nonorthogonal local-orbital (FPLO) minimum-basis scheme within the local-density approximation (LDA).²⁸ In these scalar relativistic calculations, we used the exchange and correlation potential of Perdew and Wang.²⁹ Ti $3s, 3p, 4s, 4p, 3d$ states and Be $2s, 2p, 3d$ were included as valence states. All lower states were treated as core states. We included the relatively extended semicore $3s, 3p$ states of Ti as band states because of the considerable overlap of these states on nearest neighbors. This overlap would be otherwise neglected in the FPLO method. Be $3d$ states were added to increase the quality of the basis set. The spatial extension of the basis orbitals, controlled by a confining potential $(r/r_0)^4$, was optimized to minimize the total energy.

The self-consistent potentials were carried out on a mesh of 50 k points in each direction of the Brillouin zone, which corresponds to 3107 k points in the irreducible zone. A careful sampling of the Brillouin zone is necessary to account

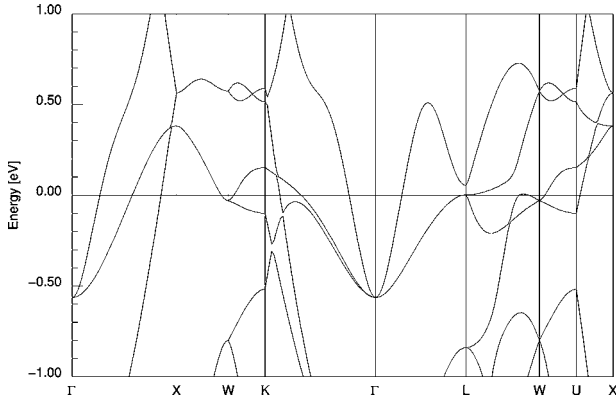


FIG. 3. Band structure of nonmagnetic TiBe_2 of Fig. 2 on an expanded scale near Fermi level. The flat bands along L - W - U / K - L lines (the hexagonal face of the fcc Brillouin zone) give rise to the density of states structure discussed in the text.

carefully for the fine structures in the density of states near Fermi level E_F . For the more delicate numerical integrations, band energies were extracted from FPLO in a mesh of 360 k points in each direction. A separate tool was developed to extract energy isosurfaces with gradients from the scalar energy grid. The isosurfaces were then used to calculate density of states and velocity moments.

To check carefully the fine structure that we will discuss, we also repeated several calculations with the general potential linearized-augmented plane wave (LAPW) method,³⁰ as implemented in the WIEN2K code.³¹ Relativistic effects were included at the scalar relativistic level. However, we verified that the magnetic moment with the experimental structure is not sensitive to the inclusion of the spin-orbit interaction. For the generalized gradient approximation (GGA) calculations, we used the exchange-correlation functional of Perdew, Burke, and Ernzerhof.³² We choose the muffin-tin spheres $R_{MT}=2.6$ a.u. for Ti, $R_{MT}=2.1$ a.u. for Be, and a basis set determined by a plane-wave cutoff of $R_{MT}K_{max}=7.0$, which gives good convergence. The Brillouin zone samplings were done using the special k point method with 1280 points in the irreducible zone.

IV. RESULTS AND DISCUSSIONS

For orientation, we first show the full nonmagnetic band structure of TiBe_2 in Fig. 2, which is consistent with earlier calculations of Refs. 23–25. The Be $2s$ bands lie between -8 eV and -2 eV. Above them the bands are of mixed s,p character, centered on the Be as well as the Ti site. Near the Fermi level, there are several bands with weak dispersion, being of primarily Ti $3d$ character. The bands at K and L are hybridized strongly, while at X the s,p character is the main character. As noted also by Jarlborg and Freeman,^{23,24} one band at L falls extremely close to E_F (3 meV below). This band is doubly degenerate along Γ - L , and the L point forms the maximum of band 15 and a saddle point for band 16. As the Fermi energy rises (for added electrons, say) the Fermi surface sweeps through the L point saddle, where the band has a vanishing velocity by symmetry. This vanishing veloc-

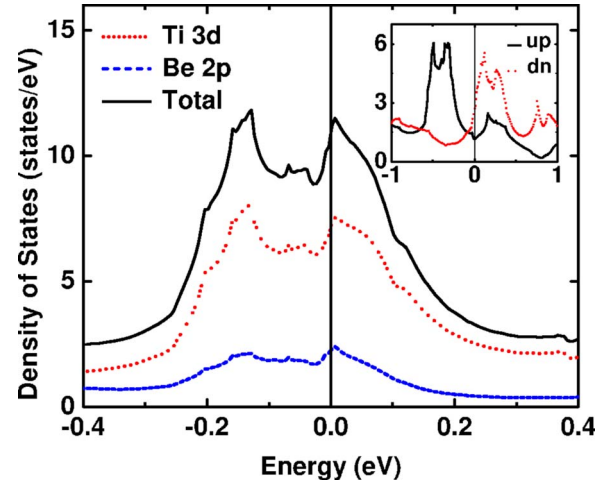


FIG. 4. (Color online) The total and atom-projected density of states (Ti, short-dashed line; Be, the lower, long-dashed line) for nonmagnetic TiBe_2 per primitive cell. The inset gives the density of states for the ferromagnetic TiBe_2 showing the exchange splitting 0.6 eV. The peak of the DOS for the majority spin is entirely below the Fermi level while that of the minority spin is above the Fermi level.

ity is discussed below. There is another doubly degenerate band very near E_f at the W point (Fig. 3).

The density of states (DOS) is shown near E_F in Fig. 4. The Fermi energy E_F falls extremely close to the edge of a very narrow peak in the DOS. The DOS peak arises from Ti d bands hybridized with Be p states. Flat bands close to Fermi level centered mostly in regions near the L - W - U and W - K directions, i.e., the hexagonal faces of the Brillouin zone, cause the sharp peak. Stewart *et al.*¹³ measured the linear specific heat coefficient for TiBe_2 of $\gamma=42$ mJ/K² mole (f.u.). The calculated value of $N(E_F)=5.33$ states/eV/f.u. for TiBe_2 corresponds to a bare value $\gamma_o=12.6$ mJ/K² mole (f.u.), leading to a thermal mass enhancement $1+\lambda=3.3$, or $\lambda=2.3$ arising from phonons, magnetic fluctuations, and Coulomb interactions.

Density functional calculations are usually reliable in calculating the instability to ferromagnetism. The enhanced susceptibility³³ is given by

$$\chi(T) = \frac{\chi_0}{1 - N(E_F)I} \equiv S\chi_0, \quad (1)$$

where $\chi_0 = \mu_B^2 N(E_F)$ is the bare susceptibility obtained directly from the band structure and I is the Stoner exchange interaction constant. Here $N(E_F)$ refers to both spins, and henceforward, we quote susceptibility in units where $\mu_B \equiv 1$. The calculation of I is from fixed spin moment calculations,³⁴ in which the energy $E(m)$ is calculated subject to the moment being constrained to be m . The behavior at small m is $E(m) = (1/2)\chi^{-1}m^2$ from which $I=0.22$ eV can be extracted from Eq. (1). This value of I gives $IN(E_F)=1.2$, larger than unity and very close to that calculated earlier,²⁴ corresponding to a Stoner ferromagnetic instability.

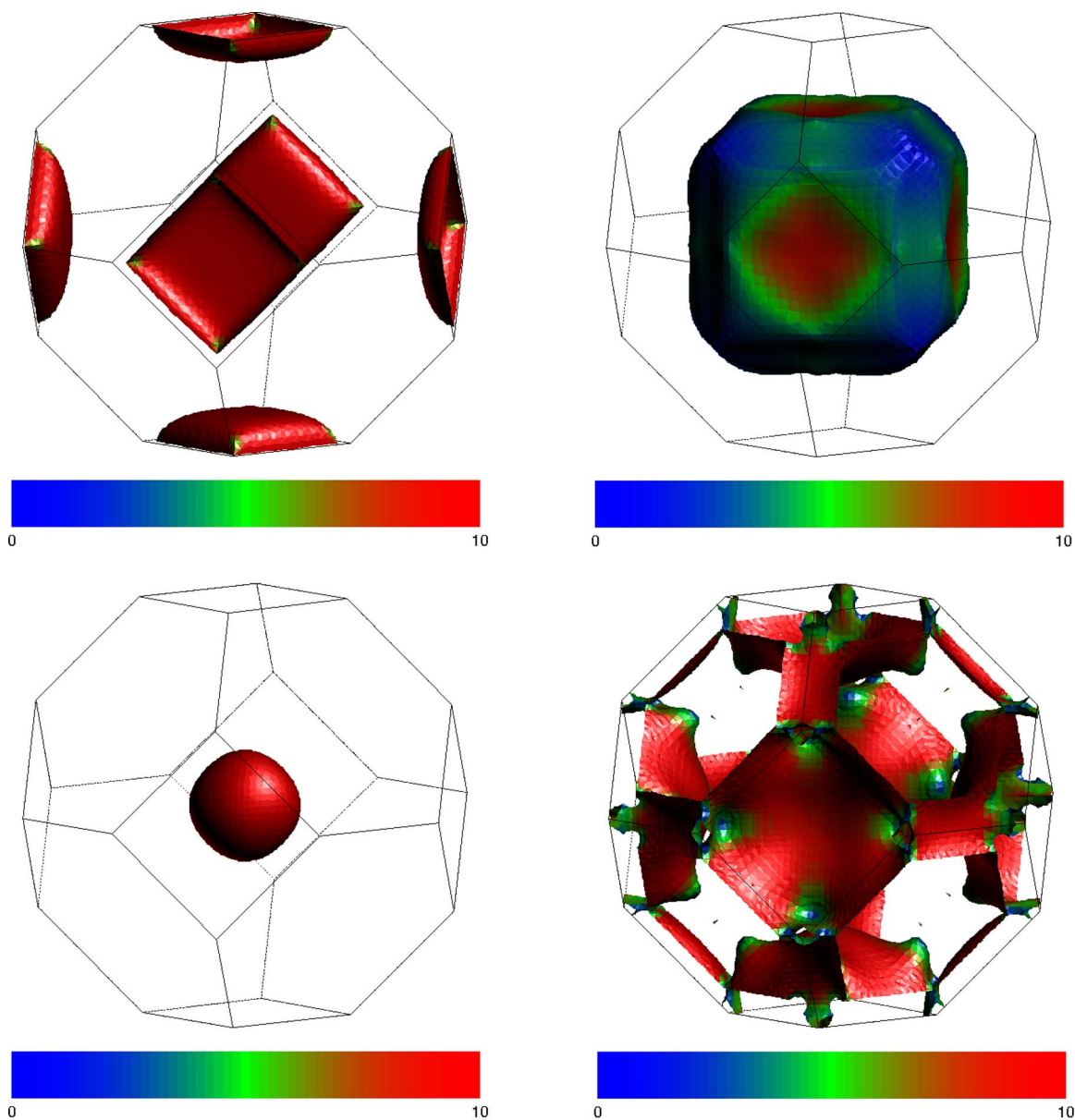


FIG. 5. (Color online) Fermi surfaces, top left: band 14, X -centered pillows; bottom right, band 15, primarily X -centered jungle gym; top right, band 16, Γ -centered pseudocube; bottom left band 17, Γ -centered sphere. Fermi velocities colored dark (blue) for lowest to lighter (red) for highest. Magnitudes of velocities are discussed in Sec. IV A.

As for a few other compounds, TiBe_2 is incorrectly predicted by LDA to be ferromagnetic. Since spin-orbit coupling is small in $3d$ magnets, we neglect it, so the direction of magnetic polarization is not coupled to the lattice. We have calculated the magnetic moment of TiBe_2 varying methods and choices of exchange-correlation functional (FPLO using LDA, LAPW using LDA, LAPW using GGA) and obtained $1.02 \pm 0.05 \mu_B$ per formula unit. This value is considerably larger than an earlier calculation²³ (which also reported a much smaller value for ZrZn_2 than obtained from more recent calculations³⁵) and apparently is due to the shape restrictions on the density and potential in the previous work. We address the overestimate of the tendency to magnetism below.

A. Fermi surface and Fermi velocity

In Fig. 5, we show the nonmagnetic Fermi surfaces shaded by the Fermi velocities. The position of E_F near L and W points sensitively determines the exact shape of some Fermi surfaces. The shapes can be characterized as (a) small Γ -centered electron sphere from band 17, (b) large Γ -centered electron pseudocube from band 16, (c) multiply connected surface mostly enclosing holes around the X point from band 15, which we refer to as the jungle gym, and (d) flat hole pillows centered at each of the three X points. The doubly degenerate bands crossing E_F along Γ - X and X - W guarantee touching of certain surfaces along these lines.

The DOS peak at and above E_F is due to the band near the L point, where the cube-shaped surfaces are about to form

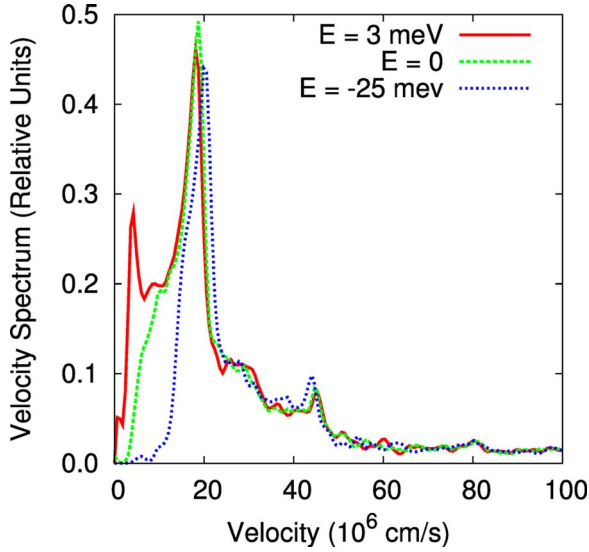


FIG. 6. (Color online) Fermi velocity spectrum of TiBe₂. The low Fermi velocity states are the primary source of changes to the density of states.

bridging necks. Figure 6 shows how the Fermi velocity spectrum $[N(V;E)]$ changes with energy at the peak just above E_F , at E_F , and at the first minimum below E_F . The Fermi velocity spectrum is defined as

$$N(V;E) = \sum_{\vec{k}} \delta(E_{\vec{k}} - E) \delta(V_{\vec{k}} - V) = \int_{\mathcal{L}(V;E)} \frac{d\mathcal{L}_{\vec{k}}}{|\vec{v}_{\vec{k}} \times \nabla_{\vec{k}}|\vec{v}_{\vec{k}}|}, \quad (2)$$

with normalization $\int N(V;E)dV = N(E)$. Here $\mathcal{L}(V;E)$ is the line of intersection of the constant energy $E_{\vec{k}} = E$ surface with the constant velocity surface $|\vec{v}_{\vec{k}}| = V$. The gradient of the velocity in the denominator makes this distribution delicate to calculate accurately. $N(E, V)$ was calculated numerically by extracting a triangulated energy isosurface from the band structure, then obtaining a velocity histogram of the states associated with the isosurface.

The spectrum in Fig. 6 shows, at E_F , velocities extending down to the very low value of 2×10^6 cm/s, and up to 5×10^7 cm/s, a variation of a factor of 25. Roughly half of the weight lies below 10^7 cm/s. At the van Hove singularity at +3 meV, the only noticeable difference is additional velocities extending down to zero due to the vanishing velocity at L (we have not worried about reproducing the $V \rightarrow 0$ behavior precisely). At -25 meV, which is just below the narrow peak at E_F , the strong weight in the spectrum appears only at 7×10^6 cm/s. Note that there is very little change in the high velocity spectrum over small changes in energy.

V. ANALYSIS OF VELOCITY DISTRIBUTION AND SUSCEPTIBILITY

A. Renormalization due to spin fluctuations

Following the work of Larson *et al.*³⁶ for Pd which builds on Moriya theory, we first attempted to identify the relevant band characteristics in order to evaluate the spin fluctuation

reduction of χ in TiBe₂. For this, one begins with the bare susceptibility in the small q and small ω limit, given by

$$\chi_0(\vec{q}, \omega) = N(E_F) \left[1 - A \left(\frac{qa}{2\pi} \right)^2 + i \frac{1}{2} \left\langle \frac{1}{v} \right\rangle_F \frac{\omega}{q} \right], \quad (3)$$

while the screened susceptibility using the random phase approximation (RPA) is given by

$$\chi^{-1}(\vec{q}, \omega) = \chi_0^{-1}(\vec{q}, \omega) - I. \quad (4)$$

The Moriya parameter $A = -7.2$, expressed in dimensionless form here, and mean inverse Fermi velocity $\langle 1/v \rangle_F \equiv v_F^{-1}$ (the second Moriya parameter, discussed below) are derived from velocity moments and DOS of the band structure, and like the density of states, they are greatly influenced by the Fermi surface topology and its velocity spectrum. Specifically, changes in topology which give rise to points of zero velocity in the band structure near the Fermi surface become an important factor. The mean inverse Fermi velocity which governs the imaginary part of $\chi_0(\vec{q}, \omega)$ is given by

$$\left\langle \frac{1}{v(E)} \right\rangle \equiv v^{-1}(E) = \frac{\sum_k \frac{\delta(\varepsilon_k - E)}{|\vec{v}_k|}}{\sum_k \delta(\varepsilon_k - E)} \quad (5)$$

evaluated at E_F . The difference between $\langle v^{-1} \rangle_F$ and $1/\langle v \rangle_F$ is one measure of the velocity variation of the Fermi surface. The bottom or top of a three-dimensional band (corresponding to the appearance or vanishing of a Fermi surface) gives only a discontinuity proportional to the square of the band mass. At a saddle point, such as the merging of the corners of the pseudocube Fermi surfaces, $v^{-1}(E)$ undergoes a $1/\sqrt{E - E_{cr}}$ divergence because the associated Fermi surface area does not vanish. This ‘‘van Hove singularity’’ in $v^{-1}(E)$ is evident for the band edge 3 meV from E_F in TiBe₂ in Fig. 7. We calculated $\langle 1/v_F \rangle^{-1} = 1.8 \times 10^7$ cm/s for TiBe₂.

For cubic structures, the parameter A in Eq. (3) is given by

$$A = \frac{1}{48\pi e^2} \left(\frac{2\pi}{a} \right)^2 \frac{d^2 \Omega_p^2(E_F)}{dE_F^2},$$

$$\Omega_p^2(E_F) = \frac{4\pi e^2}{3} \sum_k \vec{v}_k^2 \delta(\varepsilon_k - E_F) \equiv \frac{4\pi e^2}{3} N(E_F) v_F^2. \quad (6)$$

Thus, A is proportional to the second derivative of the square of the Drude plasma energy Ω_p (i.e., \hbar is absorbed into Ω_p , so Ω_p here explicitly has energy units; k sums are understood to be normalized over the zone). The second moment of velocity is finite everywhere, but its second derivative is not (for example, for free electrons this diverges as the band edge). Derivatives have the unfortunate property of amplifying noise in numerical evaluations. We have addressed the noise issue by using a large number of k points in the numerical integration ($360 \times 360 \times 360$). By fitting $\Omega_p(E)^2$ with a polynomial near the Fermi energy, we obtain the above-mentioned value $A = -7.2$. The Fermi velocity was calculated to be $v_F = 4.7$ eV bohr = 3.7×10^7 cm/s.

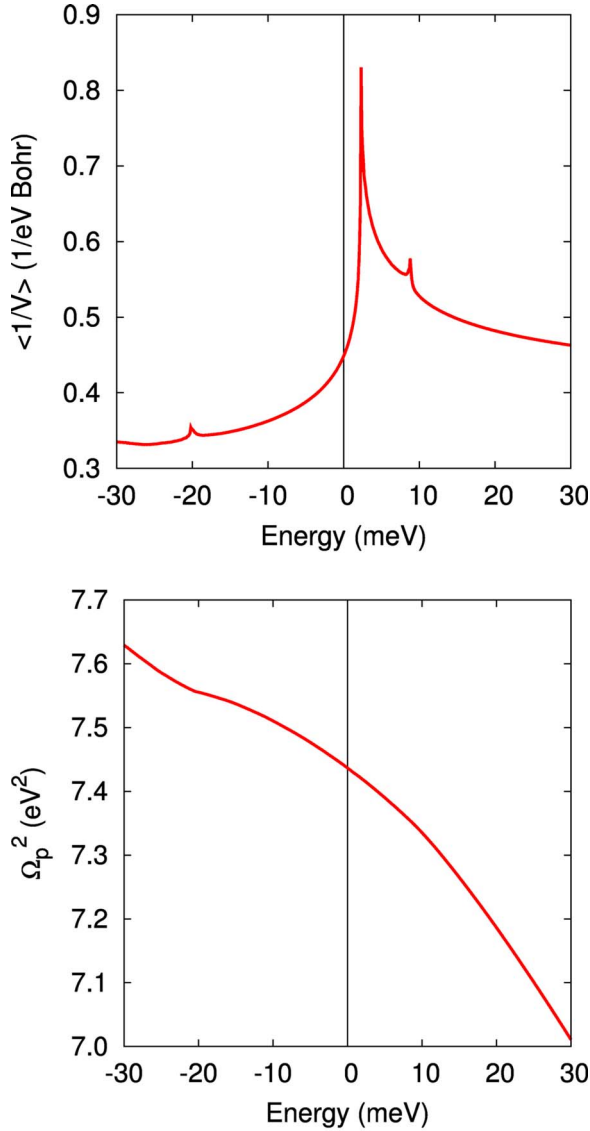


FIG. 7. (Color online) Top panel: $\langle 1/v(E) \rangle$ plotted versus energy, showing the square root divergence of the inverse moment of velocity near the Fermi energy. Unit conversion is 1 eV Bohr $\approx 8 \times 10^6$ cm/s. Bottom panel: the graph of the second moment of velocity (with constants included to show it as the square of the Drude plasma energy) is concave downward, which gives rise to the negative value of the Moriya A parameter. This sign of A is verified by the calculation of $\chi(q)$ at small q (see text).

B. q -dependent susceptibility

The negative value of the A parameter indicates, from Eq. (3), that the primary magnetic instability in TiBe₂ does *not* lie at $q=0$ but rather at finite q , so it is more susceptible to antiferromagnetic (AF) instability (including possibly a spin spiral) rather than ferromagnetic. The sign of A has been verified independently by explicit calculation of the real part of $\chi(\vec{q})$, with results shown in Fig. 8.

The calculation of $\chi_{\alpha\beta}(\vec{q})$ between bands α and β was performed by an isosurface slicing method. The susceptibil-

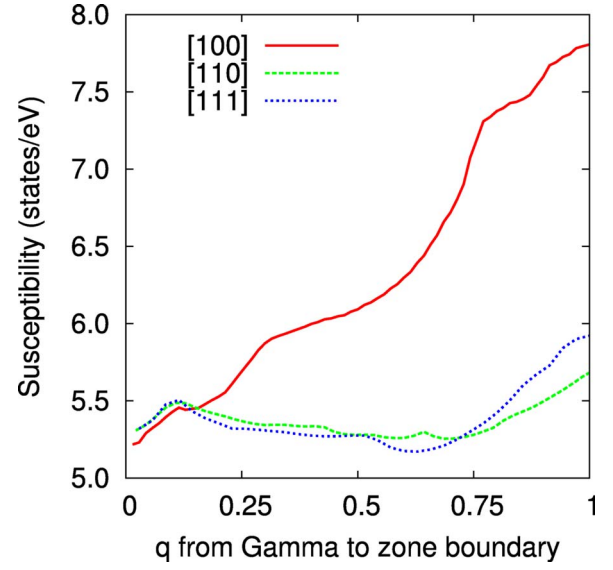


FIG. 8. (Color online) Intraband contribution to the real part of $\chi(\vec{q})$. The increase at small q confirms the sign of Moriya A coefficient (see text). Although both [110] and [111] directions have a maximum at the zone boundary, the peak along [100] (X point of the zone) dominates the instability.

ity can be written, after inserting a factor $1 \equiv \int d\Delta \delta(\Delta - \epsilon_{\beta, \vec{k}+\vec{q}} + \epsilon_{\alpha, \vec{k}})$, as

$$\chi_{\alpha\beta}(\vec{q}) = \int d\Delta \frac{N_{\alpha\beta}^X(\Delta)}{\Delta},$$

$$N_{\alpha\beta}^X(\Delta) = \sum_k [f(\epsilon_{\alpha, \vec{k}}) - f(\epsilon_{\beta, \vec{k}+\vec{q}})] \delta(\Delta - \epsilon_{\beta, \vec{k}+\vec{q}} + \epsilon_{\alpha, \vec{k}}), \quad (7)$$

where $N_{\alpha\beta}^X(\Delta)$ is a susceptibility density calculated from the isosurface defined by the Fermi functions and the energy δ function. The Brillouin zone was divided into a $140 \times 140 \times 140$ grid of cubes. Within each cube the Δ integral is calculated as a discrete sum, using variable step sizes in Δ corresponding to 1/30 of the maximum difference in energies $\epsilon_{\beta, \vec{k}+\vec{q}} + \epsilon_{\alpha, \vec{k}}$ within the cube.

The susceptibility rises equally along all three symmetry directions (as required by cubic symmetry), but only for \hat{q} along the cubic axis does $\chi(\vec{q})$ continue to increase strongly beyond the small- q region. The maximum of $\chi_o(\vec{q})$ occurs at the X point, where the intraband part has increased by nearly 50% over its $q=0$ value. In such cases, where $q=0$ is not the maximum, it is necessary to apply the extension of weak ferromagnets to the AF case.³⁷

The band-by-band contributions to $\chi_o(q)$ have been evaluated both to verify the code and to identify the source of the important contributions and structures. The sphere Fermi surface (FS) gives rise to a Lindhard type form with $2k_F \approx \pi/a$ (but is not perfectly round). The pillows lead to a cusp for $(q_x, 0, 0)$ for $q_x \approx 0.28\pi/a$, and along all three directions decreases for $q \geq \pi/a$. For the jungle gym and the pseudocube, χ increases by a factor of 2 at the zone boundary along $(q_x, 0, 0)$, with much less variation in the other two directions. The contributions to $N(E_F)$ from each of the

bands is as follows: sphere, 1.4%; pillows, 7%; jungle gym, 33%; pseudocube, 58%.

Away from $q=0$, the interband contributions to $\chi(q)$ contribute, and it is known in other transition metals and their compounds that the \vec{q} dependence of matrix elements can be important. We have calculated also the interband $\chi(\vec{q})$ for several bands around the Fermi level, finding that they contribute a broad maximum at intermediate $|q|$. It seems unlikely, however, that interband contributions will move the maximum away from the X point.

Peaking of $\chi(\vec{q})$ at the zone boundary implies a short wavelength $\lambda=a$ AF instability (incipient, since no AFM phase is observed). With the fcc lattice and two Ti atoms in the primitive cell, there several possibilities for the most unstable mode, which will involve antialignment of spins or charge density wave variation, but also may involve noncollinear alignment of the spins. We have tried to obtain a $q=0$ AFM state within LDA, with atomic moments antialigned on the bipartite Ti lattice, but the moment vanished when this was tried. We have not investigated possible $\vec{q}=X$ point AFM states.

C. Temperature dependence of susceptibility

The high narrow peak in the DOS near E_F suggests an explanation of the T dependence of χ mentioned in Sec. I, or at least part of it. To understand what part arises from simple thermal smearing, we have evaluated

$$N(E, T) \equiv \int_{-\infty}^{\infty} \left[-\frac{\partial f[E - \mu(T)]}{\partial E} \right] N(E) dE, \quad (8)$$

where the chemical potential $\mu(T)$ is adjusted at each temperature to keep the number of electrons (occupied states) constant. This temperature smearing has occasionally been addressed in the past, for example, for ZrV_2 .³⁸ The result is shown in the upper panel of Fig. 9 as a series of curves for T ranging from 0 to 300 K. It is necessary to include the variation in μ , and the value of $N[\mu(T), T]$ decreases by 8%.

The resulting change in the physical, enhanced susceptibility is given by

$$\chi(T) = \frac{N[\mu(T); T]}{1 - IN[\mu(T); T]}. \quad (9)$$

Adjusting I to reproduce the peak height (at 10 K, experimentally), which requires $I=0.183$ eV [$S=56$ at the maximum of $N(\mu)$], the resulting enhanced $\chi(T)$ is compared with the data in the lower panel of Fig. 9. It is evident that this simple temperature smearing accounts for much of the observed temperature dependence. Additional indirect temperature smearing will come from phonons and from electronic and magnetic interactions as these excitations are increasingly excited upon raising the temperature. We conclude that TiBe_2 contains no appreciable contribution to the susceptibility from local moments.

D. Field dependence of susceptibility

For an energy-dependent DOS and a highly enhanced susceptibility, a field-dependent susceptibility $\chi(H, T=0)$

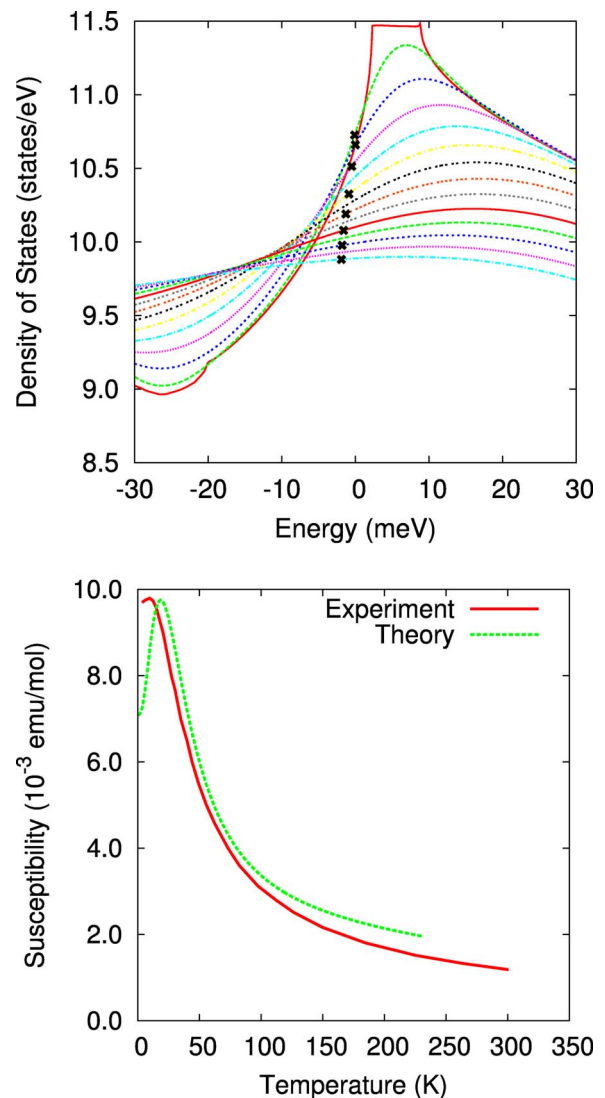


FIG. 9. (Color online) The upper graph shows how the density of states near the Fermi energy changes from $T=0$ to $T=300$ K. The lower graph shows the experimental susceptibility³⁹ compared to theory. The Stoner I has been adjusted slightly from the calculated value to match the susceptibility maximum.

$\equiv \chi(H)$ is expected. In TiBe_2 , a strong effect of this kind has been seen, which can be characterized as field-driven ferromagnetism. The differential susceptibility $\chi_d(H) = d\mathcal{M}(H)/dH$, where \mathcal{M} is given by the difference in electron occupations $n_\sigma(H)$. A many-body treatment shows that the spin imbalance can be expressed⁴⁰ in terms of the spin-dependent thermal (energy E surface averaged) Green's function,

$$G_\sigma(E, i\omega_n; H) = \frac{1}{i\omega_n - (E - \mu - \sigma\mu_B H) - \Sigma_\sigma(H)},$$

$$n_\sigma(H) = \int dE N(E) T \sum_i G_\sigma(E, i\omega_n; H) e^{i\omega_n \eta}, \quad (10)$$

here, ω_n is the fermionic Matsubara discrete energy variable and η is a positive infinitesimal. The simplest form of

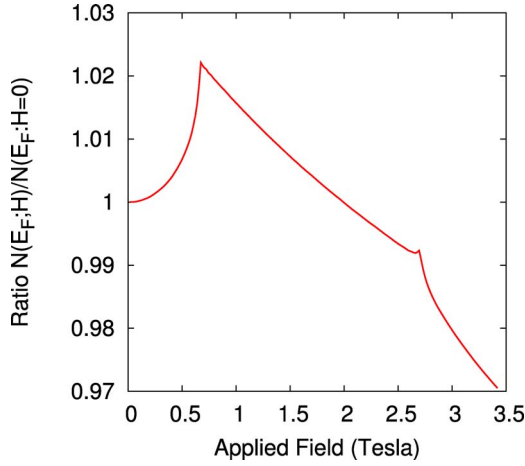


FIG. 10. (Color online) Magnetic field (H) dependence of the Fermi level density of states for TiBe_2 , referred to its $H=0$ value, as defined in the text. The initial increase with field indicates an increasing instability toward ferromagnetic order.

(Stoner) self-energy $\Sigma_{\sigma} = \sigma K \mu_B H$ should be appropriate ($1 + K = S$).

Taking the field derivative of $\mathcal{M}(H)$ but keeping H finite, and using (in this approximation)

$$G_{\sigma}(E, i\omega_n; H) = G_0[E - \sigma \mu_B(1 + K)H, i\omega_n; H=0], \quad (11)$$

we obtain the result at zero temperature

$$\chi_d(H) = \frac{d\mathcal{M}(H)}{d(\mu_B H)} = S[N(E_F - S\mu_B H) + N(E_F + S\mu_B H)]. \quad (12)$$

This clearly reduces to the usual $T=0$ result at $H=0$. A slightly better treatment would have also some H dependence of S due to the structure in $N(E)$ and the delicate situation here that $IN(E_F)$ is approaching unity, but at this point we neglect such details.

The result for the relative correction

$$\mathcal{R} = \frac{N(E_F - S\mu_B H) + N(E_F + S\mu_B H)}{2N(E_F)} \quad (13)$$

is shown in Fig. 10. The effect on the ratio (thus on the differential susceptibility) is clear; however, even with the factor of $S=60$ enhancement of the energy scale ($\mu_B H \rightarrow S\mu_B H$), the peak occurs at a field one order of magnitude smaller than seen in experiment. This difference seems to indicate that the field influence on the spin fluctuations dominates; however, the variation in $N(E)$ will need to be accounted for in any quantitative explanation.

VI. SUMMARY

The complex and sometimes confusing data on the enhanced paramagnet TiBe_2 were discussed in Sec. I. It seems clear that treatment of magnetic fluctuations will be required to understand the underlying mechanisms that suppress magnetic order. Here, we have presented a precise calculation

and analysis of the electronic structure of TiBe_2 , especially focusing on the Fermi surfaces and velocity spectrum at and near the Fermi level that underlies not only the single-particle excitations but also the spectrum of magnetic fluctuations in the itinerant limit, which seems to be the case in TiBe_2 .

Our calculations have confirmed the sharp structure in the density of states around the Fermi level that had been noted earlier and have quantified the tiny energy scale that is involved: the Fermi level lies in a region of steep DOS, just 3 meV from an abrupt van Hove singularity. This singularity is derived from a doubly degenerate band at the L point of the zone. We have provided a method for calculating the spectrum of velocities (speeds) over the Fermi surface and find the spectrum to be peaked at (the low value of) 10^7 cm/s, with much of the weight lying below that value. Moriya theory for weak ferromagnets requires, for the imaginary part of the inverse susceptibility, the moment $\langle 1/v_F \rangle$; we have illustrated that $1/v(E)$ diverges at the van Hove singularity signaling possible problems with applying Moriya theory to TiBe_2 .

Moriya theory for weak ferromagnets also requires the dimensionless quantity $A \propto d^2\Omega_p(E)/dE^2$ at the Fermi energy, where Ω_p is the conventional transport Drude energy. We find that this quantity is not positive, as it must be for an incipient ferromagnet; rather it is negative indicating that the dominating (nearby) magnetic instability is finite q : antiferromagnetic, spin wave, spin spiral, etc. Direct calculation of the generalized susceptibility $\chi_o(q)$ confirms the sign of A , and reveals the dominant instability to lie at the X point of the Brillouin zone, making TiBe_2 an incipient antiferromagnet. This result is not inconsistent with the observed onset of ferromagnetism at 15% replacement of Be with Cu, because the Fermi level will have moved to a new position in energy with its own spectrum of velocities.

We have shown that the sharp structure in $N(E)$ has other consequences for the interpretation of data on TiBe_2 . First, it leads to a T -dependent chemical potential. Together with the temperature broadening of $N(E)$ and the Stoner enhancement $S \approx 60$, simple thermal broadening can account for most if not all of the temperature dependence of the susceptibility, which some investigators had interpreted as Curie-Weiss-like. As a result, the occurrence of local moments in TiBe_2 can be ruled out. Similarly, we have shown that this sharp structure in $N(E)$, again together with the large Stoner enhancement, has a substantial effect on the field dependence of the differential susceptibility. There is still the question of how much of the measured field dependence is due to this induced exchange splitting, and how much is due to the effect of the field on the magnetic fluctuations.

Many of the results we have obtained here are strongly dependent on details of the band structure and the position of the Fermi level. That these results reflect realistically the mechanisms underlying the many fascinating observations obviously requires that the band structure formalism is applicable in detail to such systems and that the calculations are accurate. Another requirement is that of high sample quality, that the stoichiometry is precise and that defect concentration

must be very low (simple impurity broadening will affect behavior). These questions must be addressed in deciding whether to press onward to a more complete and more challenging explanation that includes effects of both magnetic fluctuations and the energy dependence of the density of states.

ACKNOWLEDGMENTS

We acknowledge illuminating communications with Z. Fisk, I. I. Mazin, G. R. Stewart, and D. J. Singh about weak ferromagnetism and materials issues. This work was supported by DOE Grant No. DE-FG03-01ER45876.

-
- ¹H. Saji, T. Yamada ya, and M. Asama, *J. Phys. Soc. Jpn.* **21**, 255 (1966).
- ²B. T. Matthias, A. L. Giorgi, V. O. Strobinger, and J. L. Smith, *Phys. Lett.* **69A**, L441 (1978).
- ³V. C. Rakhecha, G. P. Fletcher, S. K. Singh, J. L. Smith, and B. T. Matthias, *Solid State Commun.* **33**, 495 (1980).
- ⁴S. Teacake, H. Asoka, C. Y. Huang, and J. L. Smith, *J. Phys. Soc. Jpn.* **50**, 2137 (1981).
- ⁵F. Acker, Z. Fisk, J. L. Smith, and C. Y. Huang, *J. Magn. Magn. Mater.* **22**, 250 (1981).
- ⁶P. Monod, I. Felner, G. Ghouteau, and D. Shaltiel, *J. Phys. (France) Lett.* **41**, L551 (1980).
- ⁷D. Shaltiel, P. Monod, and L. Felner, *J. Phys. (France) Lett.* **41**, L-567 (1980).
- ⁸E. P. Wohlfarth and P. Rhodes, *Philos. Mag.* **7**, 1817 (1962).
- ⁹E. P. Wohlfarth, *J. Magn. Magn. Mater.* **20**, 77 (1980).
- ¹⁰F. Acker, R. Huguenin, M. Pelizzone, and J. L. Smith, *Phys. Rev. B* **24**, R5404 (1981).
- ¹¹C. J. Shinkel, F. R. de Boer, and B. de Hon, *J. Phys. F: Met. Phys.* **3**, 1463 (1973).
- ¹²A. P. J. van Deursen, A. R. de Vroomen, and J. L. Smith, *Solid State Commun.* **36**, 305 (1980).
- ¹³G. R. Stewart, B. T. Matthias, A. L. Giorgi, E. G. Szklarz, and J. L. Smith, *Solid State Commun.* **30**, 709 (1979). The structure in the specific heat at 2 K was an experimental artifact [G. R. Stewart (private communication)].
- ¹⁴G. S. Knapp, F. Y. Fradin, and H. V. Culbert, *J. Appl. Phys.* **42**, 1341 (1971).
- ¹⁵P. G. Mattocks and D. Melville, *J. Phys. F: Met. Phys.* **8**, 1291 (1978).
- ¹⁶C. Pfeleiderer, M. Uhlarz, S. M. Hayden, R. Vollmer, H. v. Lohneysen, N. R. Bernhoeft, and C. G. Lonzarich, *Nature (London)* **412**, 58 (2001).
- ¹⁷E. A. Yelland, S. M. Hayden, S. J. C. Yates, C. Pfeleiderer, M. Uhlarz, R. Vollmer, H. v. Lohneysen, N. R. Bernhoeft, R. P. Smith, S. S. Saxena, and N. Kimura, *Phys. Rev. B* **72**, 214523 (2005).
- ¹⁸G. R. Stewart, J. L. Smith, and B. L. Brandt, *Phys. Rev. B* **26**, 3783 (1982).
- ¹⁹D. M. Ioshpe, *Mod. Phys. Lett. B* **5**, 721 (1991).
- ²⁰M. Shimizu, *Proc. Phys. Soc. London* **86**, 147 (1965).
- ²¹A. A. Povsner and D. V. Likhachev, *Int. J. Mod. Phys. B* **9**, 1171 (1995).
- ²²T. Moriya and K. Ueda, *Rep. Prog. Phys.* **66**, 1299 (2003).
- ²³T. Jarlborg, A. J. Freeman, and D. D. Koelling, *J. Magn. Magn. Mater.* **23**, 291 (1981).
- ²⁴T. Jarlborg and A. J. Freeman, *Phys. Rev. B* **22**, 2332 (1980).
- ²⁵R. A. de Groot, D. D. Koelling, and F. M. Mueller, *J. Phys. F: Met. Phys.* **10**, L235 (1980).
- ²⁶A. Aguayo and D. J. Singh, *Phys. Rev. B* **66**, 020401(R) (2002).
- ²⁷A. Aguayo, I. I. Mazin, and D. J. Singh, *Phys. Rev. Lett.* **92**, 147201 (2004).
- ²⁸K. Koepernik and H. Eschrig, *Phys. Rev. B* **59**, 1743 (1999); H. Eschrig, *Optimized LCAO Method and the Electronic Structure of Extended Systems* (Springer, Berlin, 1989).
- ²⁹J. P. Perdew and Y. Wang, *Phys. Rev. B* **45**, 13244 (1992).
- ³⁰D. J. Singh, *Planewaves, Pseudopotentials, and the LAPW Method* (Kluwer Academic, Boston, 1994).
- ³¹P. Blaha, K. Schwarz, G. K. H. Madsen, D. Kvasnicka, and J. Luitz, *WIEN2k, An Augmented Plane Wave + Local Orbitals Program for Calculating Crystal Properties* (K. Schwarz, Tech. University Wien, Austria, 2001); J. P. Perdew and Y. Wang, *Phys. Rev. B* **45**, 13244 (1992).
- ³²J. P. Perdew, K. Burke, and M. Ernzerhof, *Phys. Rev. Lett.* **77**, 3865 (1996).
- ³³J. F. Janak, *Phys. Rev. B* **16**, 255 (1977).
- ³⁴K. Schwarz and P. Mohn, *J. Phys. F: Met. Phys.* **14**, L129 (1984).
- ³⁵I. I. Mazin and D. J. Singh, *Phys. Rev. B* **69**, 020402(R) (2004).
- ³⁶P. Larson, I. I. Mazin, and D. J. Singh, *Phys. Rev. B* **69**, 064429 (2004).
- ³⁷T. Moriya and K. Ueda, *Rep. Prog. Phys.* **66**, 1299 (2003) provides a recent summary on this subject.
- ³⁸B. M. Klein, W. E. Pickett, D. A. Papaconstantopoulos, and L. L. Boyer, *Phys. Rev. B* **27**, 6721 (1983).
- ³⁹W. Gerhardt, J. S. Schilling, H. Olijnyk, and J. L. Smith, *Phys. Rev. B* **28**, 5814 (1983).
- ⁴⁰W. E. Pickett, *Phys. Rev. Lett.* **48**, 1548 (1982); *Phys. Rev. B* **26**, 1186 (1982).